Ceramics International xxx (xxxx) xxx

Contents lists available at ScienceDirect

Ceramics International

journal homepage: www.elsevier.com/locate/ceramint

Growth behavior of energy-efficient protective black flash-PEO coatings on additively manufactured aluminum–silicon alloys

Muhammad Ahsan Iqbal *, Endzhe Matykina, Itziar Hidalgo-González, Raul Arrabal, Marta Mohedano

Departamento de Ingeniería Química y de Materiales, Facultad de Ciencias Químicas, Universidad Complutense de Madrid, 28040, Madrid, Spain

ARTICLE INFO

Handling Editor: Dr P. Vincenzini

Keywords:
Additive manufacturing
Plasma electrolytic oxidation
Black PEO
Energy consumption
EIS

ABSTRACT

The energy-efficient flash-PEO (plasma electrolytic oxidation) approach is being investigated to develop thin black protective PEO coatings on Al10SiMg alloys fabricated through SLM (selective laser melting). The effects of various Flash-PEO treatment durations, ranging within 2–5 min, were investigated in an electrolyte composed of phosphate, Na-EDTA, and sodium hydroxide, with ammonium metavanadate added as a coloring additive. The correlation among the coating composition, black coloration, and corrosion resistance performance was examined via structural analysis, energy consumption during the process, and EIS analysis. The findings indicate that treatment duration, up to the limit of 4 min, substantially influences the development of VOx compounds that demonstrate the black hue, with the color transition occurring between 2 and 4 min. However, extending the treatment time beyond this limit yielded no further enhancements in color intensity or corrosion resistance. Furthermore, the coating demonstrated an energy consumption of 1–2 kW h m^{-2}·μm^{-1}, increasing the system's hardness by up to five orders of magnitude relative to the bare substrate, yielding $|Z|_{10mHz}$ 3×10^4 Ω cm^2 after 10 days of immersion in 3.5 wt% NaCl solution, while retaining up to 90 % of its ΔE (blackness).

1. Introduction

Additive manufacturing (AM) has rapidly emerged as an effective approach for manufacturing complex material components and expediting the materials revolution, which has been hindered by traditional production processes [1,2]. Aluminum–silicon (Al–Si) alloys with great machinability, minimum dimensional shrinkage, high fluidity, and good weldability have been shown to have significant applications in additive manufacturing [3,4]. However, their limited tribological performance, poor corrosion resistance and inadequate hardness hinder their application in scenarios requiring extended service life. Surface treatment has become an essential strategy for enhancing the performance of aluminum alloys. Among the various functional coatings, black surface coatings with high light absorption and infrared radiation are receiving significant attention because of their ability to improve the competitiveness of aluminum components for aerospace and optical applications, in addition to providing enhanced corrosion protection. Black coatings for aluminum alloys have been developed through various processes, including organic paints, chemical conversion, electroplating, and anodic oxidation [5–9], with a growing need for innovative coating techniques that meet stringent environmental regulations, minimum energy consumption, and improve performance under harsh conditions.

Plasma electrolytic oxidation (PEO) has recently gained interest for the development of black coatings on Mg, Ti, and Al alloys because of its high emittance, strong coating/substrate adhesion, and superior corrosion resistance properties [10–15]. PEO coatings are produced through electrochemical oxidation process, wherein metal oxides form through simultaneous inward and outward growth from the substrate surface. This mechanism creates a strong metallurgical bond at the substrate/coating interface, delivering excellent adhesion and structural integrity that significantly enhances performance and enhances the coating's durability [16]. Recent studies have focused on understanding how process variables and electrolyte concentration influence the coating color and thermal control characteristics of black PEO coatings [17–21]. However, plasma electrolytic oxidation (PEO) is characterized by high energy consumption, with typical treatment times ranging from 15 to 60 min, and operates at current densities and voltages between 10 and 60 A dm^{-2} and between 200 and 400 V, respectively [22–24]. Table 1 provides a comparison of the general conditions reported in the literature regarding the development of black PEO coatings on

* Corresponding author.
E-mail address: miqbal@ucm.es (M.A. Iqbal).

https://doi.org/10.1016/j.ceramint.2025.02.280
Received 30 November 2024; Received in revised form 9 February 2025; Accepted 19 February 2025
Available online 19 February 2025

Table 1
Black PEO coatings on aluminum base alloys under different conditions reported in the literature.

Substrate	Electrolyte	Additive	Treatment Conditions	Coloring Analysis[a]	Corrosion resistance	Ref
Al-12Si	$(NaPO_3)_6$,	NH_4VO_3	100 mA/cm^2 ≥ 800 s	As prepared: N/A Postcorrosion: N/A	N/A	[25]
1060 Al	$(NaPO_3)_6$, NaOH	NH_4VO_3, Na_2WO_4	20 min at 900 Hz frequency and 20 % duty cycle with a constant current density of 150 mA/cm^2.	As prepared: α_s ~ 90 % Postcorrosion: N/A	N/A	[26]
Al-Si alloy	$(NaPO_3)_6$, NaOH	NH_4VO_3, Na_2WO_4	100–400 V negative voltage was fixed at 30 V 1 kHz, and the duty ratio was 30 %. All the samples were PEO treated for 14 min.	L = 31.51, a = 1.37, b = 0.5 Post corrosion: N/A	N/A	[18]
6061 Al	Na_2SiO_3 NaOH	$VOSO_4$	50 Hz 10 A dm^{-2} 10 min	As prepared: N/A, $\alpha_s/\varepsilon_{IR}$ ratio ≈1.0 Post corrosion: N/A	N/A	[27]
7075 Al	Na_2SiO_3 $(NaPO_3)_6$, NaOH	NH_4VO_3	Constant voltage model of 460 V/−40 V, duty cycle 40 %/−20 % 100–600 Hz	As prepared: L = 19, a = 0, b = 1 at 200 Hz Pos tcorrosion: N/A	$\|Z\\|_{0.01}$ 10^7 after 1 h in 3.5 wt% NaCl	[28]
6061 Al	$(NaPO_3)_6$, KOH	NH_4VO_3 $K_2Cr_2O_7$	Constant current of 1.8 A/cm^2 and a pulse frequency of 900 Hz upto 40 min	As prepared: α_s ~ 90 % Pos tcorrosion: N/A	–	[19]
7075 Al	3 g/L $Na_2SiO_4{\cdot}9H_2O$ + 6 g/L KOH	$(NH_4)_6Mo_7O_{24}$, K_2TiF_6, $Na_2WO_4{\cdot}2H_2O$	10 min at 1000 Hz frequency and 20 % duty cycle under a constant current density of 150 mA/cm^2	As prepared: α_s ~ 90 % Pos tcorrosion: N/A	i_{corr} (μA/cm^2) 10^{-4} to 10^{-5} in 3.5 wt% NaCl	[17]

[a] L-a-b (coloring parameters in color space model), α_s - solar absorptance, ε_{IR} - infrared emittance.

Table 2
Chemical composition of the Flash-PEO electrolyte.

Electrolyte Composition	Conductivity (μS/cm)	PEO treatment (min)	Sample
$(NaPO_3)_n$ 20 g/L, $Na_2EDTA{\cdot}2H_2O$ 28 g/L, NH_4VO_3 9 g/L, 1 g/L KOH	pH = 9.3 σ = 12.9 ± 0.02	2 3 4 5	PEO-2 PEO-3 PEO-4 PEO-5

Table 3
Coating parameters obtained under certain conditions.

Specimen	PEO thickness (μm)	Specific energy consumption, E_{PEO} (kW.h.m^{-2}.μm^{-1})
PEO-2	4.9 ± 1.3	1.03
PEO-3	5.1 ± 1.1	1.47
PEO-4	5.9 ± 1.3	2.05
PEO-5	5.8 ± 1.2	2.20

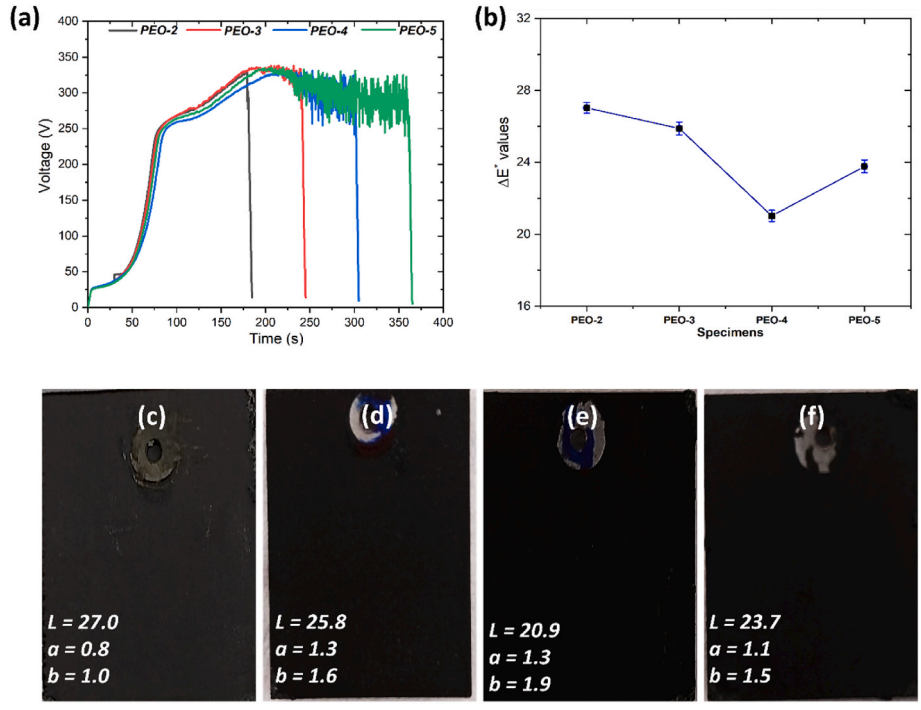

Fig. 1. (a) The variation in the voltage with time during the PEO process, (b) ΔE_0 value of the PEO, and macroscopic images of developed PEO coatings, (c) PEO-2, (d) PEO-3, (e) PEO-4, (f) PEO-5.

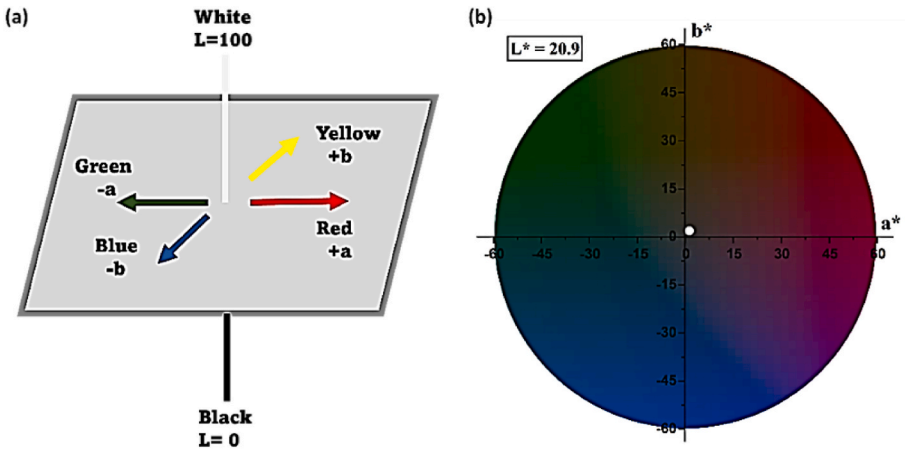

Fig. 2. Dimensional representation of the CIE Lab color model: (a) General diagram of the color model, (b) CIE Lab color model of the PEO-4 specimen. (For interpretation of the references to color in this figure legend, the reader is referred to the Web version of this article.)

aluminum alloys, highlighting that vanadate salts significantly contribute to the coloration of the coatings. It can be concluded that the energy consumption of the PEO process, corrosion protection and the stability of black color on exposure to harsh environments are critical factors for developing protective hard black coatings on an industrial scale.

Recently, the flash-PEO approach has grown into a more affordable PEO option, especially as a pretreatment strategy prior to post modification and for applications where corrosion and fatigue are more important than wear. This approach enables the deposition of thin coatings with limited treatment time under a controlled current mode [29,30]. In a recent study by *Del Olmo* et al. [29] thin functional Flash-PEO films (~5 μm) were developed with the ability to incorporate diverse corrosion inhibitors, achieving an energy consumption of 1.1–1.3 kWh m^{-2} μm^{-1} while demonstrating strong adhesion to organic systems. Although research on functional Flash-PEO coatings is limited, the technique shows significant potential for commercial applications, particularly in the aerospace sector, which demands cost-effective and environmentally friendly surface treatments. Therefore, it is crucial to identify the most effective strategies for developing functional flash-PEO coatings with durable color and corrosion protection properties. Furthermore, this work aims to address the information gap regarding the behavior of additive-manufactured (AM) substrates in the PEO process, as AM alloys have a unique microstructure that is not attainable through typical casting [31,32].

This study introduces a low-energy Plasma Electrolytic Oxidation (Flash-PEO) approach for developing vanadium oxide (VOx)-enriched coatings on aluminum substrates. The formation of black ceramic coatings highlights the tunability of the coating structure and provides insights into the relationship between PEO processing conditions, energy consumption, oxide layer morphology, and functional performance. Using NH_4VO_3 as a coloring additive, black ceramic coatings were successfully developed on additively manufactured $Al_{10}SiMg$ alloys. These findings advance the understanding of vanadium-containing black coatings and pave the way for energy-efficient, durable hard coatings capable of withstanding harsh environmental conditions.

2. Methods

2.1. Additive manufacturing of AlSi10Mg

Al10SiMg samples (50 mm × 30 mm × 2 mm) were prepared by *ERMAKSAN* (Republic of Türkiye) via selective laser melting (SLM) equipment with a 400 W fiber laser (λ = 1064 nm) and a spot size of 70 μm in a high-purity argon environment (>99.9 %). The following parameters were used to design dense samples (relative density >99.0 %): laser power: 275 W, laser spot diameter: 140 μm, layer thickness: 40 μm, and scanning speed: 0.6 m/s. The Al10SiMg powder, with a spherical shape and a mean particle diameter of 44 μm, consisted of Al (balance), Si (9.11 wt%), and Mg (0.38 wt%). The Al10SiMg powder particles were deposited with the discrete element modeling (DEM) module from Flow Science, USA, which models the powder layer on the basis of the particle size distribution and packing density (63 %).

2.2. Flash-PEO coatings

Prior to the PEO treatment, the samples were etched for 10 min at 60 °C in a 70 g/L BONDERITE C-AK 4215NC solution, then for 2 min at 40 °C in an 85 g/L BONDERITE C-AK ALUM ETCH 2 AERO solution, and finally for 5 min in BONDERITE C-IC SMUTGO NC AERO. Following each stage, the samples were washed with deionized water and dried in warm air. PEO treatments were carried out using a DC voltage/current controlled power source (SM400-AR-8 Delta Elektronika) and a current density of 100 mA cm^{-2} for various oxidation times, i.e., 2–5 min. The experimental setup included a jacketed 2 L cell with a cylindrical mesh cathode and continuous electrolyte agitation and re-circulating water at 20 °C. Ammonium vanadate (NH_4VO_3) was added to the basic electrolyte containing polymetaphosphate ($(NaPO_3)_n$, n = 5–8) and $Na_2EDTA.2H_2O$ to help develop a black coating. The electrolyte composition and coating design are shown in Table 2.

3. Characterization

The surface morphology and elemental content of the produced coatings were investigated by scanning electron microscopy (JEOL JSM-6400) with an Oxford Link energy dispersive X-ray (EDS). ImageJ was used to analyze the microporosity and pore size of the SEM images of the developed coatings, and magnification images (500 ×) were processed for quantification, followed by binarization and contrast correction. The X-ray diffraction (XRD) investigation used a Philips X'Pert diffractometer (Cu Kα 1.54 Å with a scan range of 2θ from 10 to 80°, with a scanning speed of 0.04° per second, an incidence angle of 0.5°, and a counting time of 2 s/step). The MicroRaman assessment is carried out using an NT-MDT NTEGRA Spectra spectrometer with a Solar TII MS5004i monochromator, a CCD Andor iDUS DU-420 detector (1024 × 128 pixels), and an Olympus modular BX-100 microscope with an Olympus MPlanFL 20 × /0.45NA objective. The excitation source was a 20 mW solid-state laser (filter attenuation 0.1 % ND) at a wavelength of 532 nm. The grating and acquisition periods were 600 L/mm and 300–600 s, respectively.

Surface roughness was assessed via an optical profilometer with variable focus and a × 50 magnification (Alicona InfiniteFocusSL). The

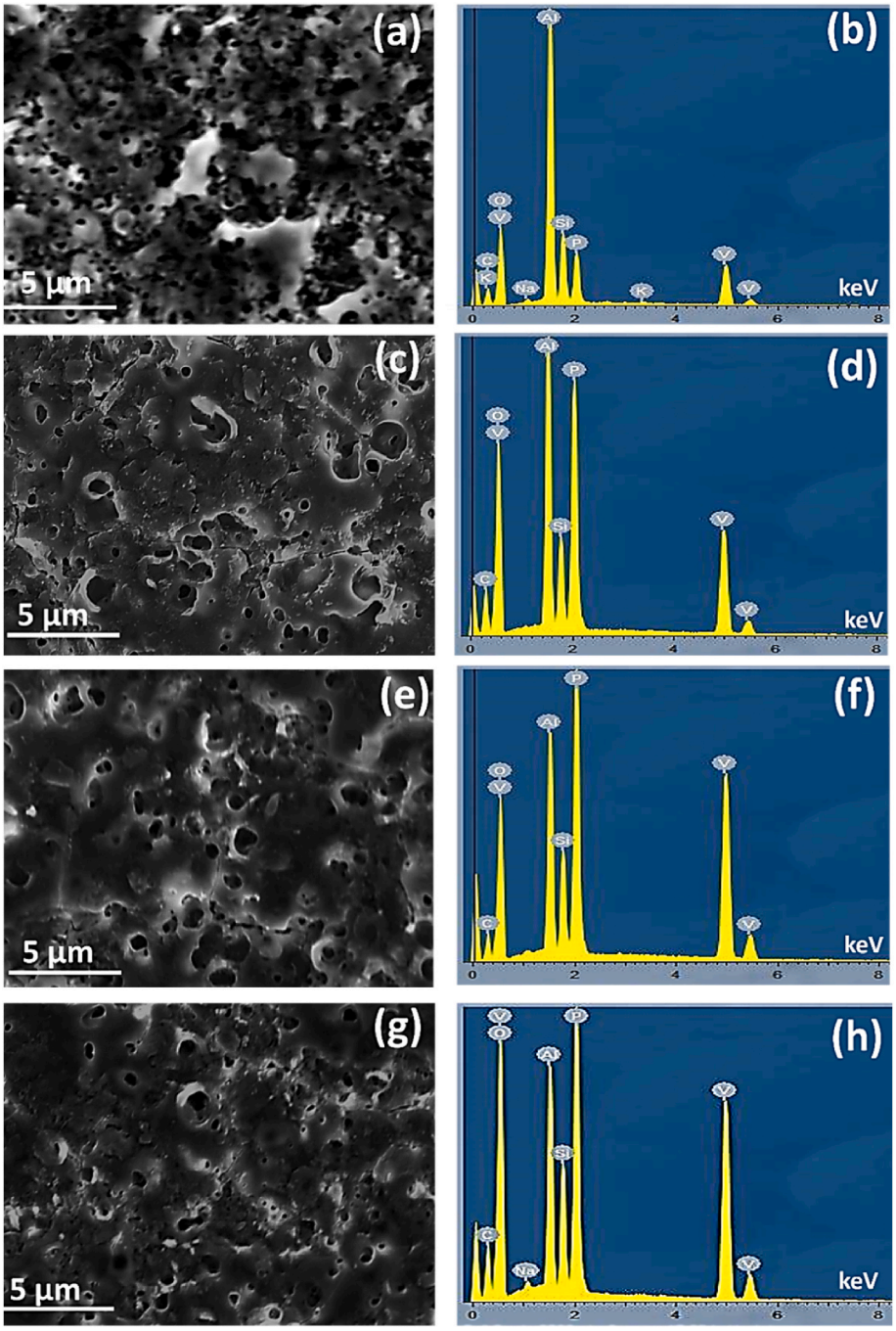

Fig. 3. SEM top views of the developed coatings and EDS spectra: (a, b) PEO-2, (c, d) PEO-3, (e, f) PEO-4, and (g, h) PEO-5.

Vickers microhardness was measured as the average of the measurements using an AKASHI MVK-E3 at a load of 10 g for 15 s. Electrochemical impedance spectroscopy (EIS) measurements were performed in a 3.5 wt% NaCl aqueous solution for up to 10 days using a typical three-electrode cell configuration associated with a GillAC computer-controlled potentiostat (ACM Instruments). The sample working area was defined as 1 cm^2, and the counter and reference electrodes were graphite and silver/silver chloride (Ag/AgCl in 3 M KCl), respectively. A sinusoidal perturbation of 10 mV amplitude was applied in the frequency range of 100 kHz to 0.01 Hz. The EIS data were analyzed via the "ZSimpWin" 3.50 program.

Optical reflectance measurements were performed with a UV–VIS–NIR spectrophotometer (UV-2600i, SHIMADZU) equipped with an integrating sphere in the 300–2000 nm range. The Cielab parameters (L, a, b) were calculated from the reflectance spectra in the 380–780 nm wavelength range.

4. Results and discussion

Fig. 1 (a) presents the voltage–time responses of the developed PEO coatings in current-controlled mode. The voltage–time response was similar for all the examined samples, with minor variations in the final voltage levels. The formation of the barrier layer on the surface was characterized by an initial voltage increase until approximately 75 s, which commenced by the oxidation of a fine silicon network up to approximately 25 s, after which the growth of the barrier Al_2O_3 layer accelerated at a steeper rate. The voltage subsequently increased at a slower rate with visible oscillations as sparking occurred during the

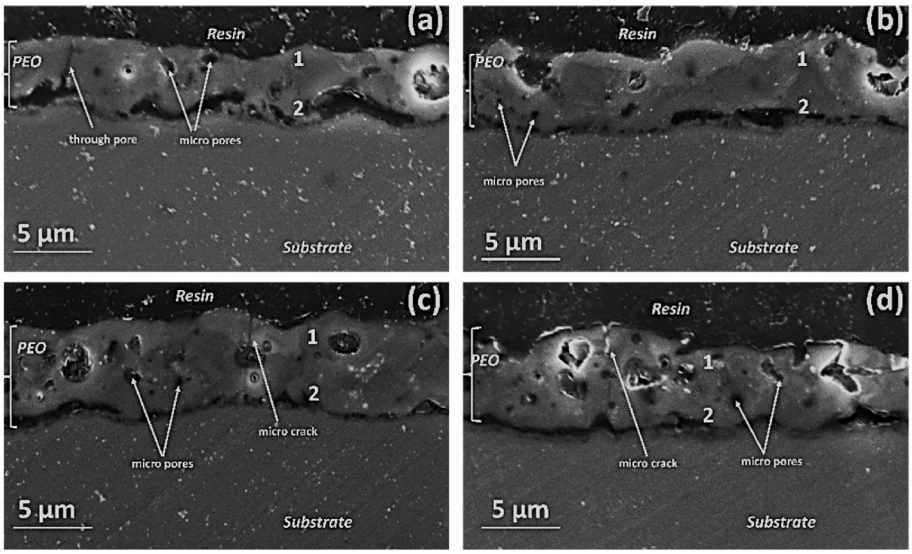

Fig. 4. Cross-sectional images of the developed PEO films: (a) PEO-2, (b) PEO-3, (c) PEO-4, and (d) PEO-5.

Table 4
The elemental composition (at. %) of the developed coatings (Figs. 3 and 4).

PEO-2	O	Al	P	V	Si
Surface (plan view)	59.0	22.8	8.4	4.3	6.8
Point 1 (outer region)	55.2	23.0	7.2	3.3	5.8
Point 2 (inner region)	52.8	37.2	4.2	1.1	2.6
PEO-3	**O**	**Al**	**P**	**V**	**Si**
Surface (plan view)	58.1	21.0	10.6	7.82	6.2
Point 1 (outer region)	55.7	28.6	9.43	6.65	5.6
Point 2 (inner)	39.7	44.7	4.58	3.20	3.2
PEO-4	**O**	**Al**	**P**	**V**	**Si**
Surface (plan view)	55.5	20.3	11.4	9.53	6.0
Point 1 (outer region)	53.4	25.4	10.33	8.94	5.7
Point 2 (inner region)	47.6	36.8	5.73	3.52	3.8
PEO-5	**O**	**Al**	**P**	**V**	**Si**
Surface (plan view)	54.0	20.4	12.7	9.3	6.0
Point 1 (outer region)	58.4	21.7	11.1	9.37	5.3
Point 2 (inner region)	58.6	27.1	5.61	3.54	3.2

formation of the PEO coatings. The developed samples exhibited an energy consumption of 1–2 kW h·m^{-2} µm^{-1}, with an obvious increase in energy consumption as the treatment time increased. Table 3 shows the measured energy consumption, thickness, and average growth rate of the PEO coatings under the investigated conditions. The oxidation time caused the color of the coating to gradually transient from grey to black with time. The coating turned strongly black after an oxidation period of ≥3 min.

The blackness of the samples was described via a CIELAB color space model. This is a three-dimensional model with three parameters, "L", "a", and "b", that correspond to a certain color. While the "a" and "b" numbers provide the color's position in the red–green and yellow–blue color coordinates, the "L" value indicates lightness (Fig. 2). The black color value can be quantified by the ΔE value (Equation (1)). The greater the black hue is, the lower the ΔE value is.

$$\Delta E = [(L)^2 + a^2 + b^2)]^{1/2} \quad \text{(Equation 1)}$$

The "L", "a", "b", and ΔE values initially decreased (strong black color) as the PEO oxidation duration increased but subsequently increased after 4 min of PEO processing. The absolute values of "a" and "b" are minimal (<2), suggesting that their coordinate geometry is extremely close to the line (L, 0, 0). This facilitates the use of the ΔE value as a measure of the PEO layer's blackness (Fig. 1 (b)). In terms of blackness, the film formed in 4 min of treatment is the best since its hue has the lowest "L" value (20.9). The Δ E values of the developed black PEO coatings are 27.03, 25.88, 21.02, and 23.76 for PEO-2, PEO-3, PEO-4 and PEO-5, respectively. The blackness of the obtained Flash-PEO coatings is promising compared with the black PEO coatings reported in the literature, considering the energy consumed during the PEO process (Table 1). Fig. 1(c–f) shows optical macrographs of the PEO-treated samples.

Fig. 3 demonstrates the surface morphology of the PEO coatings

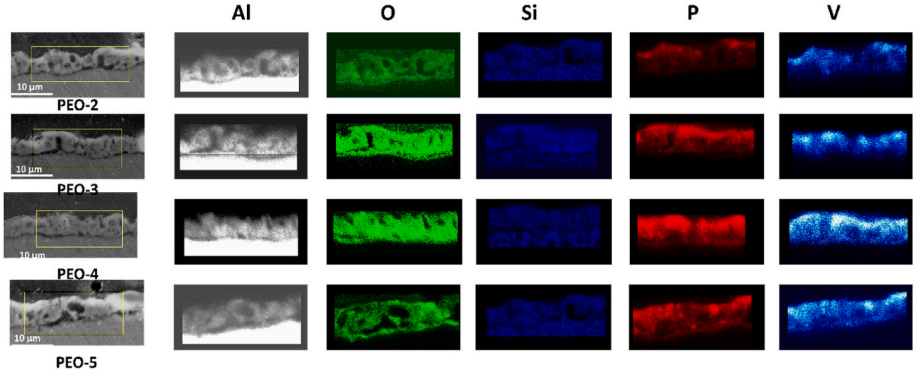

Fig. 5. SEM and EDS mapping images of developed PEO coatigs elements.

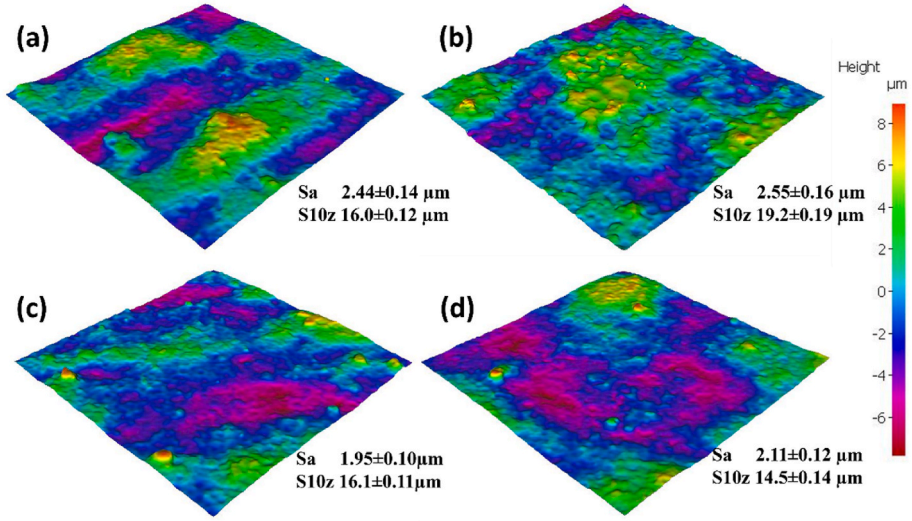

Fig. 6. Surface roughness, (a) PEO-2, (b) PEO-3, (c) PEO-4, (d) PEO-5.

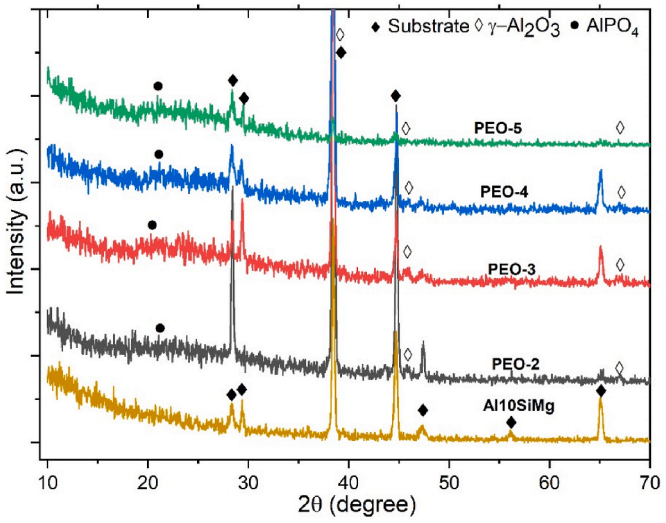

Fig. 7. X-ray diffraction patterns of the developed black PEO coatings.

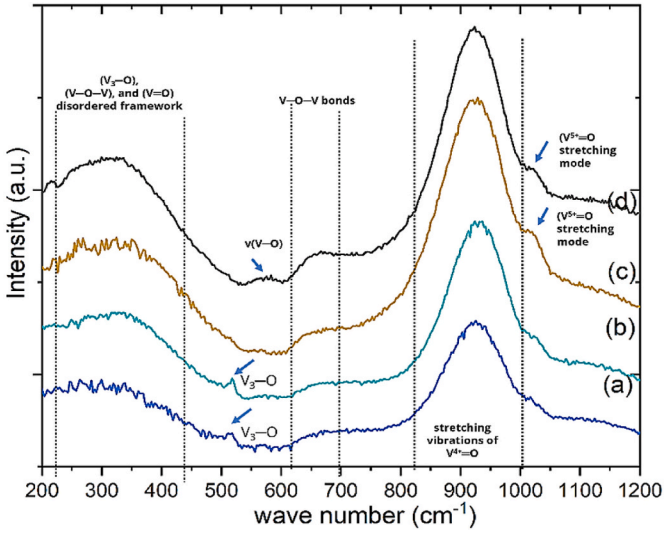

Fig. 8. Raman spectra of the developed PEO coatings: (a) PEO-2, (b) PEO-3, (c) PEO-4, and (d) PEO-5.

formed in electrolytes of various oxidation periods. The coating morphology varies with oxidation time, starting with shallow pores (PEO-2) and developing into crater-like shapes as the PEO treatment duration increases. After 2 min of oxidation, the surface morphology of the ceramic layer on the aluminum alloy resulted in micropores with circular shapes and sizes ranging from 0.1 to 0.5 μm. After 4 min of oxidation, the coating seems to be more compact, with a lower pore population density, which is also the reason for the glossier nature of PEO-4. After 5 min of treatment, the ceramic layer became coarser and more porous, with micron-sized pores (0.5–1 μm). In particular, the surfaces of PEO-4 and PEO-5 contain fewer micropores and larger pores, likely due to the development of smaller microdischarges. Increasing the processing time reduced the number of discharge channels while increasing the discharge energy, thereby producing larger pores on the coating surface and contributing to a relatively dense structure without through-thickness defects. The results further indicated a general trend where increased treatment time corresponded to a more uniform distribution of surface hills and valleys, with a reduction in surface roughness (discussed in a later section). According to the EDS spectra in Fig. 3, all PEO coatings were predominantly composed of Al, V, and O, confirming the successful incorporation of electrolyte additives into the coatings. The formation of distinct ceramic compounds on the coating surface further resulted in a gradient of colors ranging from greyish black to intense black. The PEO-4 coating exhibits the lowest porosity at 4.1 %, with an average pore area of 4.7 μm^2, as analyzed using ImageJ software. In contrast, PEO-2 shows the highest pore population density, emphasizing the impact of treatment time on micropore refinement. Meanwhile, PEO-5 displays a slight increase in porosity to 4.7 %, with defects visible on the surface and edges, and an average pore area of 5.1 μm^2.

The cross-sectional analysis and elemental distribution of PEO films were studied to better understand the role of various components in coating development. While no significant differences were observed in the ceramic layer thickness (≈5 μm), some voids or pore bands were noted at the coating/substrate interface in the PEO coatings. The coating thickness increased slightly with increasing oxidation time; however, after prolonged PEO treatment of 4–5 min, no further increase in film thickness was observed, with thicknesses ranging from 5 to 5.8 μm.

The EDS results show that the elemental distributions vary between the inner and outer layers (Table 4). Notably, a distinct compositional gradient is observed between the outer and inner layers of the PEO

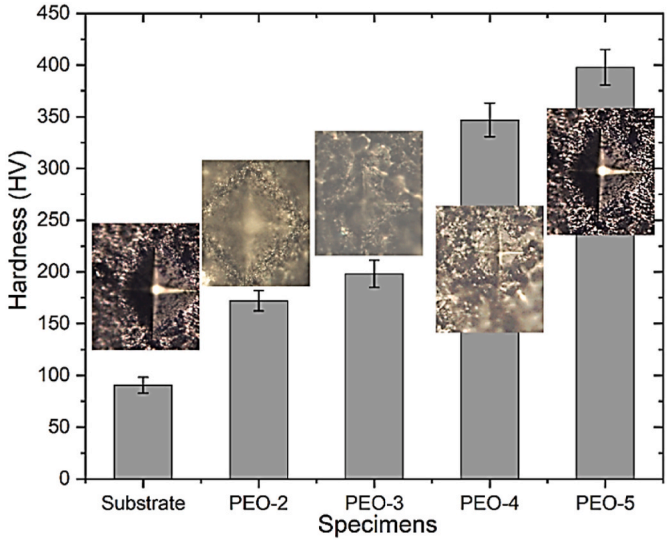

Fig. 9. Vicker hardness values of the bare substrate and PEO-treated substrate after different durations.

coatings. The amount of P (7.1–11.1 at. %) and V (3.3–9.3 at.%) in the outer layer of the oxide coating was found to be higher, while it decreased alongside the thickness (inner layer) of the PEO coating (P (4.2–5.61 at.%) and V (1.1–3.5 at.%)). In contrast, the amount of Al decreased toward the outermost layer of the coatings (due to its direct availability from the substrate). Compared with the inner layer, the outer surface has a significantly higher vanadium concentration, where the vanadium content is approximately one-third of that on the outer surface. Furthermore, in planar mode, EDS analysis revealed vanadium (V) content ranging from 4.3 at. % to 9.5 at.%, progressively increasing with extended oxidation times. This trend indicates enhanced incorporation of vanadium into the coating with extended processing durations. Furthermore, the EDS cross-sectional mapping (Fig. 5) reveals distinct compositional gradients within the coating thickness, providing valuable insights into the element distribution. The porous upper layer demonstrates a pronounced enrichment of vanadium (V) and phosphorus (P), indicating their incorporation from the electrolyte during the plasma electrolytic oxidation (PEO) process. In contrast, aluminum (Al) concentration is predominantly dense near the substrate. This inverse distribution of V and Al is consistently observed across all coatings, highlighting the outer porous and inner dense layer structure typical of PEO coatings. Notably, the optimized, black-colored specimens (i.e. PEO-4) exhibit a significantly higher vanadium concentration in the upper porous layer, correlating with their superior functional properties, including enhanced absorptivity and black color.

The influence of PEO treatment on the surface roughness was investigated further through an optical profilometer (Fig. 6). When the treatment duration was changed from PEO-2 to PEO-3, the roughness value initially increased, but a subsequent increase in oxidation time resulted in surface smoothness, with a value of Sa = 1.95 μm for PEO-4. In contrast, additional increases (PEO-5) revealed a higher value of "Sa = 2.11 μm" but a lower value than those for PEO-2 and PEO-3. The black hue of the PEO coatings appeared strong for PEO-4 and PEO-5, making them difficult to discern with the human eye; however, the surface roughness values differed slightly, i.e., within the range of 1.95–2.55 μm. Given the intensity of the observed black color (ΔE) and surface roughness, PEO-4 has the smoothest glossy surface.

According to the XRD patterns (Fig. 7), all the PEO coatings under study had $AlPO_4$ and γ-Al_2O_3 as their primary composition [33–35]. This is the typical behavior of PEO coatings on Al alloys produced in phosphate electrolytes. Previous investigations have shown that lower voltages (350–400 V) promote the synthesis of γ-Al_2O_3, whereas higher voltages (450 V) increase the possibility of developing α-Al_2O_3 [36,37]. $AlPO_4$ is formed when P_6O_{18}− hexamer anions decompose into PO_4^{3-} in a plasma environment [38]. Due to the coatings low thickness, Al peaks from the substrate were also detected. The incorporation of complex salts into the electrolyte significantly influences the crystallization behavior of the oxide layer during the Flash PEO process, suppressing the characteristic γ-Al_2O_3 reflections and broadening the XRD peaks [29]. This disruption hinders the complete crystallization of gamma alumina and the absence of distinct VOx phases, resulting in a mixed-phase structure dominated by amorphous or poorly crystalline components. Fast cooling rates of the resultant small and short-lived micro discharges at lower voltages are insufficient to promote crystallization. These findings correspond with the short treatment times and low energy consumption characteristic of the flash-PEO process, emphasizing its potential for creating amorphous oxide layers with functional properties. The broad diffraction halo observed between 2θ values of 15° and 27°, characteristic of amorphous materials, highlights the predominantly amorphous nature of the coatings, with approximately 80–85 % of the oxide layer being amorphous. This observation aligns with the elemental composition data obtained from EDS analysis, which confirms the successful incorporation of vanadium species into the amorphous matrix. Raman spectroscopy, discussed in the subsequent section, provides further validation of these findings, offering complementary evidence of the amorphous structure and the presence of vanadium oxides within the coatings.

The Raman spectra (Fig. 8), analyzed to confirm the presence of amorphous VO_x compounds, exhibited a dominant broad peak (800–1000 cm^{-1}), characteristic of the wide bands associated with a mixture of amorphous VO_x [39–41]. The broad band at 300 cm^{-1} is attributed to the bending vibrations of the triply coordinated oxygen (V3—O), doubly coordinated oxygen (V—O—V), and terminal oxygen (V=O) bonds in a disordered V—O—V framework [42–44]. Therefore, these results support the formation of VO_x compounds on the PEO surface [45]. The orthophosphate (Q_0) group is represented by a 590 cm^{-1} band for the symmetric stretching of the P-O bonds [46]. The Raman spectra of amorphous γ-Al_2O_3 exhibit week shoulder at approximately 401 cm^{-1}, which corresponds to the characteristic vibrational mode of the Al-O bond in the amorphous phase. In addition to this, several medium-intensity bands are observed in between 550 cm^{-1} and 875 cm^{-1}. These bands are indicative of the disordered structure of the amorphous oxide [47]. The amorphous nature of the deposited VO_x compounds suggests that although their concentration increases with treatment time, the low voltage and short treatment duration of the Flash-PEO process (2–5 min) are insufficient to facilitate crystallization. During PEO coating, the salt of NH_4VO_3 dissociates into NH^{4+} and VO^{3-}, which interact with the molten flux to form amorphous non-stoichiometric VO_x [48]. Li et al. [48] reported similar findings when NH_4VO_3 was used as an electrolyte in the PEO coating process of aluminum alloys. In this process, VO^{3-} ions in solution were absorbed onto the surfaces, forming an adsorption layer that reduced the surface energy of the newly formed metastable phase. This phenomenon explains the black coloration observed, which is attributed to surface defects and oxygen vacancies in VO_x compounds rather than the formation of dark green phases. Prolonging the PEO duration increased the spark energy, promoting the transformation of VO^{3-} and leading to a greater accumulation of vanadium oxides in the heat-affected zones, which progressively darkened the coating layers, transitioning from grey to black within 2–4 min. The spectral band at 666 cm^{-1} is attributed to the vibrational modes of VO_3 and is predominantly observed in the PEO-4 and PEO-5 samples [39]. The PEO-4 samples exhibited a strong black hue, and further processing did not enhance black coloration, suggesting that the mean spark energy reached a critical value beyond which no additional color variation occurred. It appears that a ~9.5 at.% vanadium content and the resultant amorphous VO_x compounds are primarily responsible for the black coloration observed in the coatings. Their disordered structure leads to broad absorption of visible light

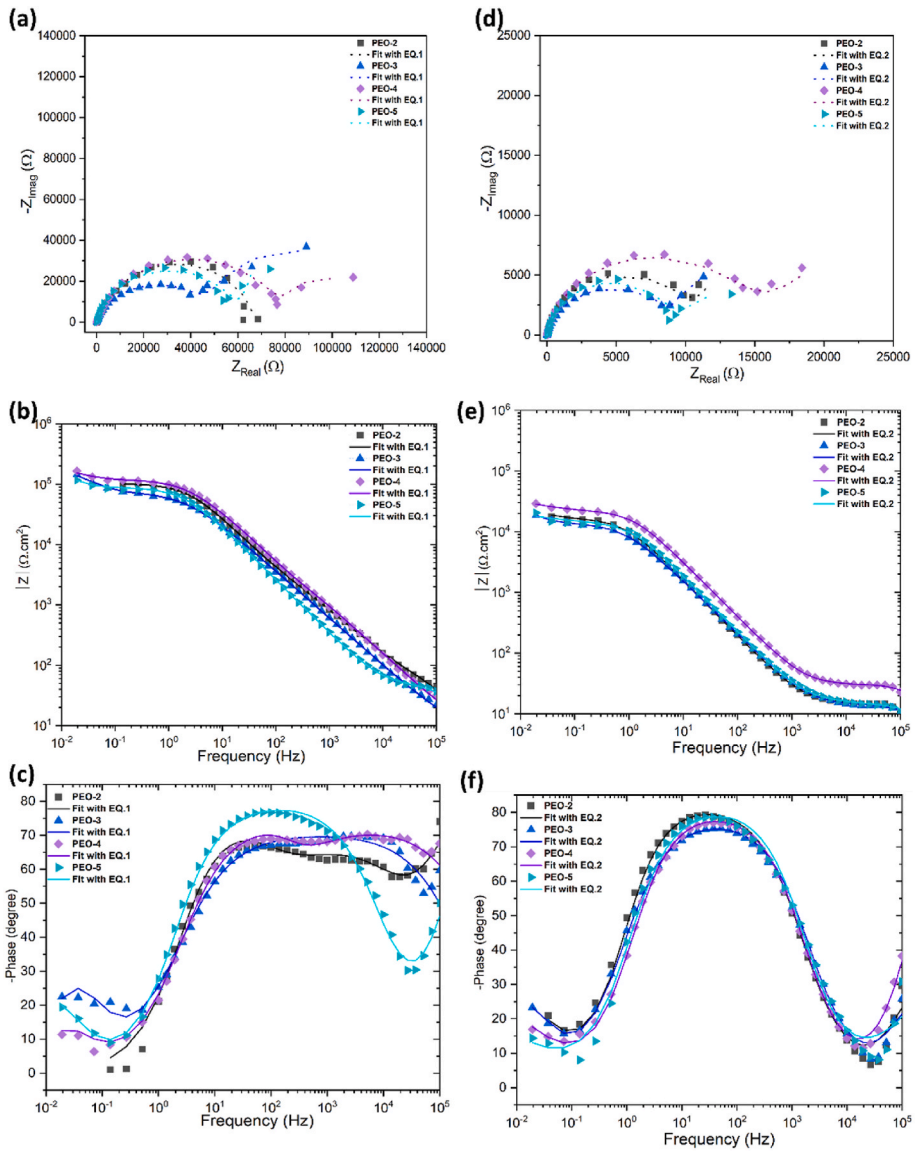

Fig. 10. EIS spectra of the developed coatings for different immersion times, (a–c) after 1 day, and (d–f) after 10 days immersion in 3.5 wt% NaCl solution.

Table 5
Evolution with time of the fitting parameters R_{out}, CPE_{out}, α_{out}, R_{in}, CPE_{in}, α_{in} R_{ct}, Q_{dl}, and α_{dl} after 24 h of immersion.

Sample	CPE_{out} Ω^{-1} cm^{-2} s^{α}	α_{out}	R_{out} Ω cm^2	CPE_{in} Ω^{-1} cm^{-2} s^{α}	α_{in}	R_{in} Ω cm^2	CPE_{dl} Ω^{-1} cm^{-2} s^{α}	α_{dl}	R_{ct} Ω cm^2
PEO-2	$3.24 \times 10^{-6} \pm 0.38 \times 10^{-6}$	1.00 ± 0.09	$4.51 \times 10^{1} \pm 0.29$	$7.85 \times 10^{-7} \pm 0.58 \times 10^{-7}$	0.91 ± 0.04	$9.41 \times 10^{4} \pm 0.15$	$4.45 \times 10^{-6} \pm 0.35 \times 10^{-6}$	0.67 ± 0.07	$2.7 \times 10^{3} \pm 0.12$
PEO-3	$1.63 \times 10^{-8} \pm 0.28 \times 10^{-8}$	0.74 ± 0.08	$6.51 \times 10^{1} \pm 0.37$	$2.09 \times 10^{-7} \pm 0.49 \times 10^{-7}$	0.89 ± 0.04	$7.75 \times 10^{4} \pm 0.26$	$6.49 \times 10^{-5} \pm 0.39 \times 10^{-5}$	0.96 ± 0.07	$1.0 \times 10^{5} \pm 0.11$
PEO-4	$8.68 \times 10^{-8} \pm 0.27 \times 10^{-8}$	0.80 ± 0.07	$1.02 \times 10^{2} \pm 0.37$	$5.47 \times 10^{-8} \pm 0.37 \times 10^{-8}$	1.00 ± 0.03	$1.12 \times 10^{5} \pm 0.29$	$1.34 \times 10^{-6} \pm 0.26 \times 10^{-6}$	1.00 ± 0.06	$6.0 \times 10^{5} \pm 0.12$
PEO-5	$2.85 \times 10^{-7} \pm 0.29 \times 10^{-7}$	1.00 ± 0.07	$5.90 \times 10^{1} \pm 0.46$	$1.68 \times 10^{-6} \pm 0.35 \times 10^{-6}$	1.00 ± 0.03	$8.99 \times 10^{4} \pm 0.18$	$1.24 \times 10^{-6} \pm 0.24 \times 10^{-6}$	0.88 ± 0.07	$8.7 \times 10^{4} \pm 0.30$

across a wide range of wavelengths, resulting in black color.

Fig. 9 shows the Vickers hardness profiles of the surface, which indicate the mechanical characteristics of the coating system. PEO coatings formed with extended oxidation times, such as PEO-4 and PEO-5, show microhardness values approximately four times higher than the bare substrate, with PEO-5 exhibiting an even greater enhancement, approximately 4.7 times that of the substrate. Although the hardness measurement includes contributions from the substrate due to the thin layer thickness, the Vickers hardness measurements show a considerable improvement in the overall hardness of the system with increasing PEO oxidation time.

The preceding discussion elucidates the considerable effect of various PEO times on additive (V) incorporation inside the surface and affects the evolution of its geometry and microstructure, all of which affect its protective efficacy. EIS data were utilized to evaluate the corrosion resistance of the produced samples in a 3.5 wt% NaCl aqueous solution. The oxide coating formed during the PEO process displayed three distinct time constants in the EIS data (Fig. 10a–d). The high-

Table 6
Evolution with time of the fitting parameters R_{out}, CPE_{out}, α_{out}, R_{in}, CPE_{in}, α_{in} R_{ct}, Q_{dl}, and α_{dl} after 240 h of immersion.

Sample	CPE_{out} Ω^{-1} cm^{-2} s^{α}	α_{out}	R_{out} Ω cm^2	CPE_{in} Ω^{-1} cm^{-2} s^{α}	α_{in}	R_{in} Ω cm^2	CPE_{dl} Ω^{-1} cm^{-2} s^{α}	α_{dl}	R_{ct} Ω cm^2	w Ω^{-1} cm^{-2} s^5
PEO-2	$1.28 \times 10^{-7} \pm 0.38 \times 10^{-7}$	1.00 ± 0.01	$1.33 \times 10^{1} \pm 0.17$	$1.34 \times 10^{-5} \pm 0.28 \times 10^{-5}$	0.97 ± 0.03	$1.36 \times 10^{4} \pm 0.15$	$4.27 \times 10^{-6} \pm 0.38 \times 10^{-6}$	0.68 ± 0.02	$1.0 \times 10^{2} \pm 0.09$	$5.0 \times 10^{-5} \pm 0.38 \times 10^{-5}$
PEO-3	$1.49 \times 10^{-7} \pm 0.21 \times 10^{-7}$	1.00 ± 0.02	$8.47 \times 10^{1} \pm 0.21$	$1.74 \times 10^{-5} \pm 0.30 \times 10^{-5}$	0.87 ± 0.04	$1.48 \times 10^{4} \pm 0.19$	$9.23 \times 10^{-6} \pm 0.28 \times 10^{-6}$	0.99 ± 0.05	$1.6 \times 10^{4} \pm 0.11$	$2.4 \times 10^{-6} \pm 0.27 \times 10^{-6}$
PEO-4	$3.77 \times 10^{-8} \pm 0.23 \times 10^{-8}$	1.000.02	$9.52 \times 10^{1} \pm 0.25$	$6.42 \times 10^{-6} \pm 0.22 \times 10^{-6}$	0.91 ± 0.03	$2.09 \times 10^{4} \pm 0.12$	$1.41 \times 10^{-6} \pm 0.17 \times 10^{-6}$	0.78 ± 0.06	$4.5 \times 10^{4} \pm 0.14$	$2.0 \times 10^{-6} \pm 0.28 \times 10^{-6}$
PEO-5	$7.78 \times 10^{-7} \pm 0.21 \times 10^{-7}$	1.00 ± 0.02	$3.48 \times 10^{1} \pm 0.19$	$6.82 \times 10^{-6} \pm 0.19 \times 10^{-6}$	0.63 ± 0.04	$1.62 \times 10^{4} \pm 0.13$	$1.19 \times 10^{-5} \pm 0.21 \times 10^{-5}$	0.91 ± 0.04	$1.4 \times 10^{4} \pm 0.13$	$5.7 \times 10^{-5} \pm 0.22 \times 10^{-5}$

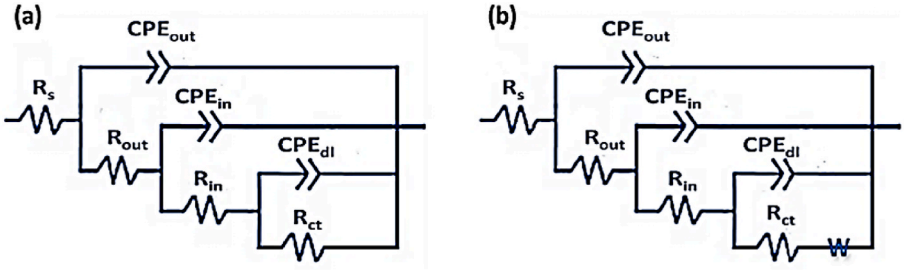

Fig. 11. Equivalent circuits used for the developed PEO coatings: (a) immersion time of 24 h and (b) immersion time of 240 h.

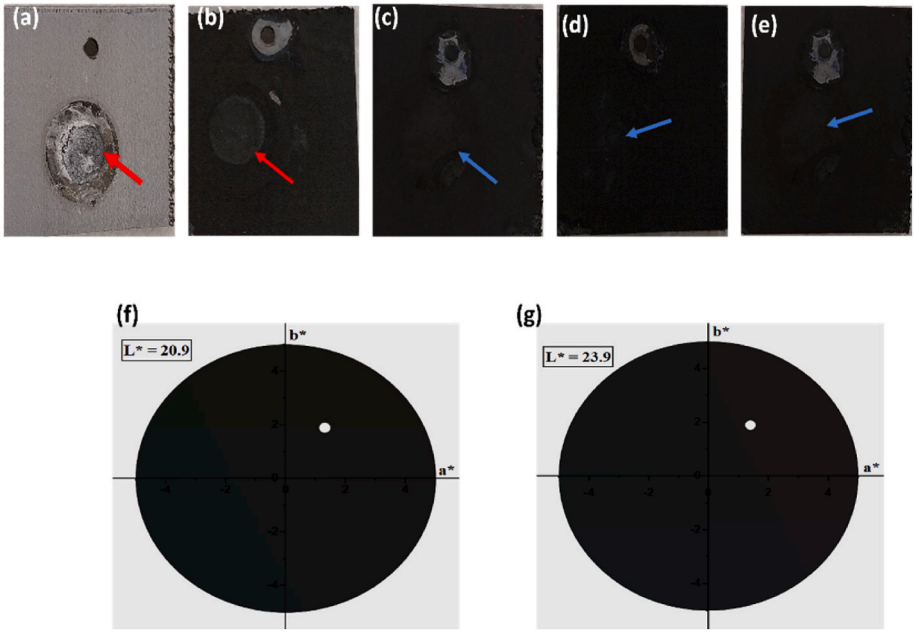

Fig. 12. Macroscopic images of the PEO-treated samples after 10 days of immersion in 3.5 wt% NaCl: (a) PEO-2, (b) PEO-3, (c) PEO-4, and (d) PEO-5; and CIE Lab color model of the PEO-4, (f) as-prepared, (g) after 10 days immersion in 3.5 wt% NaCl. (For interpretation of the references to color in this figure legend, the reader is referred to the Web version of this article.)

frequency response, characterized by the parameters (R_{out}, CPE_{out}), corresponds to the porous outer layer, while the lower-frequency response, with parameters (R_{in}, CPE_{in}), is attributed to the dense inner barrier layer. Additionally, the double-layer capacitance and charge-transfer resistance (CPE_{dl} and R_{ct}) provide insight into the electrochemical reactions occurring at the interface between the coating and corrosive agents at lower frequencies. These EIS features align well with those reported in the literature, where similar impedance behavior is observed in PEO-formed oxide coatings [49]. The high-frequency semicircle reflects the characteristics of the porous outer layer, the lower-frequency semicircle corresponds to the inner barrier layer, and the Warburg element represents the diffusion of corrosion products from the metal substrate. Overall, these findings emphasize the critical role of PEO treatment duration in shaping the oxide layer's structure and enhancing its corrosion resistance properties. After 1 day of immersion, the developed PEO coatings demonstrated the $|Z|_{10mHz}$ approximately 2

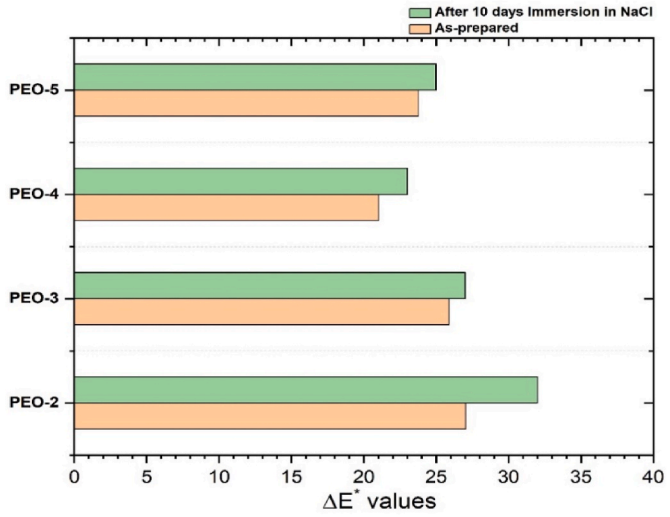

Fig. 13. The color variation (Δ E) values of the developed black flash-PEO samples before and after 10 days of immersion in a 3.5 % NaCl solution. (For interpretation of the references to color in this figure legend, the reader is referred to the Web version of this article.)

$\times 10^5$ Ω cm^2 (Fig. 10(b)). The differences in impedance magnitude among the observed samples initially are not very significant; this might be attributed to minor variations in film thickness. Further immersion in NaCl solution permits corrosive species to migrate from the outer to inner layers, resulting in the initiation of the corrosion process. After 10 days of immersion, $|Z|_{10mHz}$ decreases by approximately one order, and PEO-4 has a better impedance value (Fig. 10(e).

The EIS data (Tables 5 and 6) were further fitted via "ZSimpWin" software to analyze the corrosion resistance properties. Fig. 11 presents the corresponding equivalent circuit models for PEO-coated samples at different immersion times. After 24 h of immersion, the experimental data for the PEO coatings can be modelled with the equivalent circuit (EC) $R_s(CPE_{out}(R_{out}(CPE_{in}(R_{in}(R_{ct}CPE_{dl})))))$. For samples immersed in NaCl for 240 h, the experimental data are best modelled by a similar equivalent circuit with a Warburg diffusion coefficient (W). The Warburg coefficient is the consequence of ion diffusion from the electrolyte to the electrode interface. The quality of the fittings was assessed using chi-squared values, which ranged from 2×10^{-4} to 4×10^{-3}. These values indicate a good agreement between the experimental data and the equivalent circuit fits, suggesting that the proposed model accurately represents the electrochemical behavior of the oxide coatings under the given conditions. The well-organized geometry of PEO-4 is found to promote superior barrier characteristics, resulting in a robust protective coating over aluminium alloy against corrosion. After 240 h of immersion, the resistance ascribed to the coating's outer layer decreased drastically, caused by electrolyte penetration through cracks and defects in the oxide layer; however, the inner layer demonstrated sufficient stability (10^4 Ω cm^2). After immersion, the PEO-4 and PEO-5 coating exhibited a smooth surface, in contrast to other PEO coatings, which showed a significant accumulation of corrosive species on their surfaces (Fig. 11). The coating resistance (R_{ct}) of PEO-4 reflected the fact that this coating prevented the electrolyte from interacting with the underlying substrate more efficiently than others. During initial immersion, the R_{ct} was greater for the developed samples (10^6 Ω cm^2), but for longer PEO processing periods, it decreased to one order of magnitude (10^5 Ω cm^2), most likely because of chloride diffusion induced by a larger outer porous layer and defects in the thin layer. Compared with PEO-2 (1.81×10^4 Ω cm^2) and PEO-3 min (1.48×10^4 Ω cm^2), the PEO-4 and PEO-5 coatings developed had considerably higher R_{in} values of 2.09×10^4 Ω cm^2 and 1.62×10^4 Ω cm^2, respectively. The impedance modulus varies with immersion duration, indicating that black PEO coatings, especially for 4-min treated samples, have higher corrosion resistance compared to other black PEO. The constant phase element coefficient for the inner barrier layer, CPE_{in}, showed a relative decrease across all evaluated specimens for PEO-4, attributed to an increase in the inner barrier layer resistance. However, the CPE_{in} values for extended oxidation time (PEO-5) were slightly lower than those for PEO-4. This could be due to the relatively weaker barrier properties of PEO-5, despite its relatively similar thickness. The low barrier layer of PEO-5 was further supported by its lower impedance modulus compared to PEO-4 after initial immersion.

Macroscopic images of the substrate and developed PEO coatings after 10 days of immersion in 3.5 wt% NaCl are shown in Fig. 12. After 10 days of exposure, the substrate is severely corroded, and a thick layer of corrosive species can be observed. Owing to the strong black surface of PEO-4 and PEO-5 renders, it is difficult to identify corrosive species on the coating surface. This reveals that the color of the coating remains stable even after being exposed to a corrosive environment. The retention of VO_x compounds inside the PEO matrix during NaCl immersion ensures the functional integrity of the coating over time. This stability highlights an effective incorporation of VO_x inside the PEO matrix, ensuring prospective effectiveness and color retention (Fig. 12(f and g)). Fig. 13 presents the ΔE values (Equation (1)) corresponding to the blackness of the examined samples. Despite 10 days of immersion, the ΔE value measured in the corroded region suggested high stability of the color intensity following immersion. Although the coating developed under PEO-4 consumes slightly more energy compared to PEO-2 and PEO-3, its blackness (ΔE/2.1 (before immersion)-ΔE/2.4 (after immersion) is notably higher than that of the other specimens and exhibit superior corrosion resistance properties, while retaining the black color up to 95 % after 10 days of immersion in 3.5 % NaCl solution.

5. Conclusion

In conclusion, this study successfully developed a thin black PEO (~5 μm) coating on Al10SiMg alloy, utilizing NH_4VO_3 additives, to enhance the structural and corrosion resistance properties. The results demonstrate that increasing the oxidation time results in a color transition from grey to black, which is attributed to the increase in the amorphous VO_x content. The 4-min PEO treatment resulted in relatively high corrosion resistance and smooth glossy surface characteristics, coupled with a low energy consumption of 2.05 (kWhm^{-2}μm^{-1}) and a characteristic black color before and after immersion in NaCl. Compared to the bare substrate, the PEO coating exhibited a significant improvement in hardness, showing an increase of 4 to 4.7 times at extended oxidation times, such as for PEO-4 and PEO-5. Overall, this study highlights the potential of a flash-PEO process to achieve a balance of low energy consumption, color, and enhanced performance of coatings, particularly in terms of corrosion resistance, hardness, and retention of >90 % of blackness in terms of ΔE after 10 days of immersion. Thin black PEO coatings, characterized by their exceptional UV–Vis absorptivity, sufficient corrosion resistance, and long-lasting color stability, offer an energy-efficient solution for high-absorption applications. These properties make them particularly well-suited for environments requiring enhanced thermal management and robust protection against harsh conditions.

CRediT authorship contribution statement

Muhammad Ahsan Iqbal: Writing – original draft, Methodology, Investigation, Funding acquisition, Formal analysis, Data curation, Conceptualization. **Endzhe Matykina:** Writing – review & editing, Validation, Resources, Methodology, Conceptualization. **Itziar Hidalgo-González:** Investigation, Formal analysis, Data curation. **Raul Arrabal:** Writing – review & editing, Visualization, Validation, Conceptualization. **Marta Mohedano:** Writing – review & editing, Visualization, Validation, Supervision, Project administration,

Conceptualization.

Funding

This work is financed by the European project UNA4CAREER (Marie Skłodowska Curie grant No 847635). The authors gratefully acknowledge the support of the PID2021–124341OB-C22/AEI/10.13039/501100011033/FEDER, UE (MICIU). M. Mohedano is grateful for the support of RYC-2017-21,843 Ministerio de Ciencia e Innovación. The help of Mr. Miguel Collado Vian, supported by PEJ-2021-AI/IND-21995, Comunidad de Madrid, with PEO electrolyte optimization and Optical reflectance measurements gratefully acknowledged.

Declaration of competing interest

The authors declare that they have no known competing financial interests or personal relationships that could have appeared to influence the work reported in this paper.

References

[1] Shengyang Tang, Raghunandan Ummethala, Challapalli Suryanarayana, Jürgen Eckert, Konda Gokuldoss Prashanth, Zhi Wang, Additive manufacturing of aluminum-based metal matrix composites—a review, Adv. Eng. Mater. 23 (7) (2021) 2100053.

[2] Geir Langelandsvik, Odd M. Akselsen, Trond Furu, Hans J. Roven, Review of aluminum alloy development for wire arc additive manufacturing, Materials 14 (18) (2021) 5370.

[3] Nesma T. Aboulkhair, Marco Simonelli, Luke Parry, Ian Ashcroft, Christopher Tuck, Richard Hague, 3D printing of Aluminium alloys: additive Manufacturing of Aluminium alloys using selective laser melting, Prog. Mater. Sci. 106 (2019) 100578.

[4] R. Chou, J. Milligan, M. Paliwal, M. Brochu, Additive manufacturing of Al-12Si alloy via pulsed selective laser melting, Jom 67 (2015) 590–596.

[5] A.K. Sharma, H. Bhojraj, V.K. Kaila, H. Narayanamurthy, Anodizing and inorganic black coloring of aluminum alloys for space applications, Met. Finish. 95 (12) (1997) 14–20.

[6] Chia-Ken Leong, Yasuhiro Aoyagi, D.D.L. Chung, Carbon black pastes as coatings for improving thermal gap-filling materials, Carbon 44 (3) (2006) 435–440.

[7] Ahmed M. Awad, Maha F. Shaffei, Hala S. Hussein, Nanostructured aluminum oxide black coating: electrochemical, mechanical, and optical characterizations, J. Nanotechnol. Eng. Med. 6 (1) (2015) 011002.

[8] A.R. Shashikala, A.K. Sharma, D.R. Bhandari, Solar selective black nickel–cobalt coatings on aluminum alloys, Sol. Energy Mater. Sol. Cell. 91 (7) (2007) 629–635.

[9] Vishal Saxena, R. Uma Rani, A.K. Sharma, Studies on ultra high solar absorber black electroless nickel coatings on aluminum alloys for space application, Surf. Coating. Technol. 201 (3–4) (2006) 855–862.

[10] Wenbin Tu, Zhunda Zhu, Xiujuan Zhuang, Yingliang Cheng, Peter Skeldon, Effect of frequency on black coating formation on AZ31 magnesium alloy by plasma electrolytic oxidation in aluminate-tungstate electrolyte, Surf. Coating. Technol. 372 (2019) 34–44.

[11] Anju M. Pillai, A. Rajendra, A.K. Sharma, Parthasarathi Bera, S. Poornima, S. Sampath, Development of vanadium impregnated flat absorber composite PEO coating on AA6061 alloy, Surf. Coating. Technol. 410 (2021) 126891.

[12] Zhongping Yao, Bing Hu, Qiaoxiang Shen, Aoxiang Niu, Zhaohua Jiang, Peibo Su, Pengfei Ju, Preparation of black high absorbance and high emissivity thermal control coating on Ti alloy by plasma electrolytic oxidation, Surf. Coating. Technol. 253 (2014) 166–170.

[13] Deyyala Madhuri, Rahul Ghosh, Mohammed Adnan Hasan, Arjun Dey, Anju M. Pillai, Murugan Angamuthu, K.S. Anantharaju, A. Rajendra, Flat Absorber Black PEO coatings on Ti6Al4V for spacecraft thermal control application, Ceram. Int. 48 (23) (2022) 35906–35914.

[14] Rui Yao, Li Yang, Zhongping Yao, Peng Zhang, Songtao Lu, Xiaohong Wu, Black PEO coating with enhanced thermal stability on titanium alloy and its thermal control properties, Surf. Coating. Technol. 429 (2022) 127934.

[15] Aihua Yi, Zhongmiao Liao, Wen Zhu, Zhisheng Zhu, Wenfang Li, Kang Li, Ken Chen, Shengkai Huang, Influence of electrolyte temperature on the color values of black plasma electrolytic oxidation coatings on AZ31B Mg alloy, Coatings 10 (9) (2020) 890.

[16] Ye-kang Wu, Zhong Yang, Rui-qiang Wang, Guo-rui Wu, Dong Chen, Dong-dong Wang, Xin-tong Liu, et al., An investigation of microstructure evolution for plasma electrolytic oxidation (PEO) coated Al in an alkaline silicate electrolyte, Surf. Coating. Technol. 351 (2018) 136–152.

[17] T. Arunnellaiappan, S. Anoop, N. Rameshbabu, Fabrication of multifunctional black PEO coatings on AA7075 for spacecraft applications, Surf. Coating. Technol. 307 (2016) 735–746.

[18] Kang Li, Wenfang Li, Guoge Zhang, Ping Guo, Preparation of black PEO layers on Al–Si alloy and the colorizing analysis, Vacuum 111 (2015) 131–136.

[19] Yuting Hao, Zuoyan Ye, Minheng Ye, Hui Dong, Lili Wang, Yunchen Du, Construction and growth of black PEO coatings on aluminum alloys for enhanced wear and impact resistance, Ceram. Int. 49 (18) (2023) 30782–30793.

[20] S. Shrestha, P. Shashkov, B.D. Dunn, Microstructural and thermo-optical properties of black Keronite PEO coating on aluminium alloy AA7075 for spacecraft materials applications, in: Proc.'10th Intl. Symposium on Materials in a Space Environment', 2006, pp. 19–23. Collioure, France.

[21] Xiaorui He, Tian Feng, Yulin Cheng, Panfeng Hu, Zhengzhou Le, Zihua Liu, Yingliang Cheng, Fast formation of a black inner α-Al2O3 layer doped with CuO on Al–Cu–Li alloy by soft sparking PEO process, J. Am. Ceram. Soc. 106 (11) (2023) 7019–7042.

[22] E. Matykina, R. Arrabal, M. Mohedano, B. Mingo, Jorge Gonzalez, Angel Pardo, M. C. Merino, Recent advances in energy efficient PEO processing of aluminium alloys, Trans. Nonferrous Metals Soc. China 27 (7) (2017) 1439–1454.

[23] Muhammad Ahsan Iqbal, Endzhe Matykina, Raul Arrabal, Marta Mohedano, Role of anodic precursor layer thickness on PEO coatings: energy consumption and long-term corrosion performance, Surf. Coating. Technol. 476 (2024) 130186.

[24] E. Matykina, R. Arrabal, A. Pardo, M. Mohedano, B. Mingo, I. Rodríguez, J. González, Energy-efficient PEO process of aluminium alloys, Mater. Lett. 127 (2014) 13–16.

[25] Hwang In Jun, Duck Young Hwang, Yong Min Kim, Bongyoung Yoo, Hyuk Shin Dong, Formation of uniform passive oxide layers on high Si content Al alloy by plasma electrolytic oxidation, J. Alloys Compd. 504 (2010) S527–S530.

[26] Jinlong Pan, Yanwei Wen, Lili Wang, Zhiyong Wu, Hui Dong, Zuoyan Ye, Doping and defects: the coloring mechanism of black plasma electrolytic oxidation (PEO) films on aluminum alloys, Surf. Coating. Technol. 431 (2022) 128035.

[27] Anju M. Pillai, A. Rajendra, A.K. Sharma, Parthasarathi Bera, S. Poornima, S. Sampath, Development of vanadium impregnated flat absorber composite PEO coating on AA6061 alloy, Surf. Coating. Technol. 410 (2021) 126891.

[28] Mingyu Zhu, Yingwei Song, Zihe Liu, Dongsheng Xu, Kaihui Dong, En-Hou Han, Optimization of thermal control and corrosion resistance of PEO coatings on 7075 aluminum alloy by frequency alteration, Surf. Coating. Technol. 446 (2022) 128797.

[29] R. Del Olmo, M. Mohedano, P. Visser, E. Matykina, R. Arrabal, Flash-PEO coatings loaded with corrosion inhibitors on AA2024, Surf. Coating. Technol. 402 (2020) 126317.

[30] Ewa Wierzbicka, Marta Mohedano, Endzhe Matykina, Raul Arrabal, Design and multidimensional screening of flash-PEO coatings for Mg in comparison to commercial chromium (VI) conversion coating, Metals 11 (2) (2021) 337.

[31] L. Pezzato, C. Gennari, M. Franceschi, K. Brunelli, Influence of silicon morphology on direct current plasma electrolytic oxidation process in AlSi10Mg alloy produced with laser powder bed fusion, Sci. Rep. 12 (1) (2022) 14329.

[32] Luca Pezzato, Manuele Dabalà, Katya Brunelli, Microstructure and corrosion properties of PEO coatings produced on AM-aluminum alloys, Key Eng. Mater. 813 (2019) 298–303.

[33] S. Stojadinovic, R. Vasilic, I. Belca, M. Petkovic, Bećko Kasalica, Z. Nedic, Lj Zekovic, Characterization of the plasma electrolytic oxidation of aluminium in sodium tungstate, Corros. Sci. 52 (10) (2010) 3258–3265.

[34] Ping Wang, Ting Wu, You Tao Xiao, Jun Pu, Xiao Yang Guo, Effects of Ce (SO4) 2 concentration on the properties of micro-arc oxidation coatings on ZL108 aluminum alloys, Mater. Lett. 182 (2016) 27–31.

[35] N. Xiang, R.G. Song, C. Wang, Q.Z. Mao, Y.J. Ge, J.H. Ding, Formation of corrosion resistant plasma electrolytic oxidation coatings on aluminium alloy with addition of sodium tungstate species, Corrosion Eng. Sci. Technol. 51 (2) (2016) 146–154.

[36] Arash Fattah-alhosseini, Seyed Omid Gashti, Maryam Molaie, Effects of disodium phosphate concentration (Na 2 HPO 4· 2H 2 O) on microstructure and corrosion resistance of plasma electrolytic oxidation (PEO) coatings on 2024 Al alloy, J. Mater. Eng. Perform. 27 (2018) 825–834.

[37] Keqin Du, Xinghua Guo, Quanzhong Guo, Yong Wang, Fuhui Wang, Tian Ying, Effect of PEO coating microstructure on corrosion of Al 2024, J. Electrochem. Soc. 159 (12) (2012) C597.

[38] Gu Wei-Chao, Lv Guo-Hua, Huan Chen, Chen Guang-Liang, Feng Wen-Ran, Zhang Gu-Ling, Yang Si-Ze, Investigation of morphology and composition of plasma electrolytic oxidation coatings in systems of Na2SiO3–NaOH and (NaPO3) 6–NaOH, J. Mater. Process. Technol. 182 (1–3) (2007) 28–33.

[39] Petr Shvets, Olga Dikaya, Ksenia Maksimova, Alexander Goikhman, A review of Raman spectroscopy of vanadium oxides, J. Raman Spectrosc. 50 (8) (2019) 1226–1244.

[40] Ferran Ureña-Begara, Aurelian Crunteanu, Jean-Pierre Raskin, Raman and XPS characterization of vanadium oxide thin films with temperature, Appl. Surf. Sci. 403 (2017) 717–727.

[41] Dmitry S. Kharitonov, Jens Sommertune, Cem Örnek, Jacek Ryl, Irina I. Kurilo, Per M. Claesson, Jinshan Pan, Corrosion inhibition of aluminium alloy AA6063-T5 by vanadates: local surface chemical events elucidated by confocal Raman micro-spectroscopy, Corros. Sci. 148 (2019) 237–250.

[42] Ferran Ureña-Begara, Aurelian Crunteanu, Jean-Pierre Raskin, Raman and XPS characterization of vanadium oxide thin films with temperature, Appl. Surf. Sci. 403 (2017) 717–727.

[43] Chunzi Zhang, Qiaoqin Yang, Cyril Koughia, Fan Ye, Mohsen Sanayei, Shi-Jie Wen, Safa Kasap, Characterization of vanadium oxide thin films with different stoichiometry using Raman spectroscopy, Thin Solid Films 620 (2016) 64–69.

[44] Gregory T. Went, S. Ted Oyama, Alexis T. Bell, Laser Raman spectroscopy of supported vanadium oxide catalysts, J. Phys. Chem. 94 (10) (1990) 4240–4246.

[45] Zhang Shaohong, Juan Fu, Su Qiucheng, Wu Liangpeng, Li Xinjun, In situ characterization on thermal transitions of VO2 (B): toward VO2 (R) and V2O3, Rare Met. Mater. Eng. 45 (6) (2016) 1374–1380.

[46] G.I. Petrov, V.V. Yakovlev, J. Squier, Raman microscopy analysis of phase transformation mechanisms in vanadium dioxide, Appl. Phys. Lett. 81 (6) (2002) 1023–1025.

[47] Yong Liu, Bo Cheng, Kang-Kai Wang, Guo-Ping Ling, Jun Cai, Chen-Lu Song, Gao-Rong Han, Study of Raman spectra for γ-Al2O3 models by using first-principles method, Solid State Commun. 178 (2014) 16–22.

[48] Junming Li, Hui Cai, Bailing Jiang, Growth mechanism of black ceramic layers formed by microarc oxidation, Surf. Coating. Technol. 201 (21) (2007) 8702–8708.

[49] Liye Zhu, Wei Zhang, Haitao Liu, Lei Liu, Fuhui Wang, Ziping Qiao, Single dense layer of PEO coating on aluminum fabricated by "chain-like" discharges, Materials 15 (13) (2022) 4635.